Surprising Decrease in the Martian He Bulge during PEDE-2018 and Changes in Upper Atmospheric Circulation

Meredith K. Elrod[1,2], Stephen Bougher[3], Kali Roeten[3], Kenneth Arnold[1]

[1] CRESST II, University of Maryland College Park, College Park, MD, USA
[2] Planetary Environments Lab, Code 690, NASA Goddard Space Flight Center, Greenbelt, MD, USA
[3] Department of Climate and Space Sciences and Engineering, University of Michigan, Ann Arbor, MI, USA

Key Points: (140 characters)

- He collects on the dawn/night winter polar caps. Measured highest at the seasonal points (equinox and solstice).
- He bulge density was lower in Mars Year 34 during the PEDE (near northern winter solstice) than in observations during Mars Years 32 & 35.
- He is a tracer for upper atmosphere circulation and changes in the bulge indicate changes in the circulation.

Abstract (250 words)

Using the Neutral Gas and Ion Mass Spectrometer (NGIMS) on the Mars Atmosphere Volatile and Evolution spacecraft (MAVEN) we analyzed data from Mars Year (MY) 32, 34, and 35 to examine the He bulge during the northern winter solstice (Ls ~180-240) specifically focusing on the effects from the planet encircling dust event (PEDE-2018). He collects on the dawn/nightside winter polar hemisphere of the terrestrial planets (Earth, Mars, and Venus). The seasonal migration of the Martian He bulge has been observed and modeled (Elrod et al., 2017, Gupta et al., 2021). The MAVEN orbit precesses around Mars allowing for a variety of latitude and local time observations throughout the Martian year. MY32, 34 and 35 had the best possible opportunities to observe the He bulge during northern winter (Ls ~180-240). NGIMS observations during MY 32 and MY 35 revealed a He bulge on the nightside to dawn in alignment with modeling and previous publications. However, in MY 34, during the PEDE, the He bulge was not present indicating the PEDE directly impacted upper atmospheric circulation. Updates in modeling indicate changes in circulation and winds can cause He to shift further north and dawn-ward than MAVEN was able to observe. The temperature increases in the thermosphere on the nightside during the dust storm along with changes in gravity waves and eddy diffusion occurring during this event could account for this circulation change.

Plain Language Summary (200 words)

Mars is regularly subject to large dust storms that typically start during the northern winter season. Approximately every 7-10 years these large storms can merge and grow and become

planet sized dust storms that cover 80-95% or the surface. These rare and massive planet sized storms last for about a month before slowly dissipating, changing not only the surface of the planet but also the structure and composition of the atmosphere. Mars has regular helium bulges that form in the cold part of the upper atmosphere (e.g., polar winter regions on the night and dawn side). Global circulation models of the atmosphere have made this helium bulge easily predictable throughout the Martian year. The MAVEN spacecraft has made observations of Helium over the course of 4 Martian years, and during the last major global dust storm, where a helium bulge should have been observed, no bulge appeared. This indicated that the winds and circulation in the upper atmosphere were disrupted during the global dust storm to much higher altitudes than previously thought. This could have implications for the broader impact of regular global dust storms on the Martian atmosphere.

1. Introduction

In late May/early June of 2018 the Mars Reconnaissance Orbiter (MRO) Mars Climate Sounder (MCS) detected the onset of a large dust storm system near the equator. This storm system grew and merged with other dust storms forming at the same time and by 3 June (Ls ~186) 2018, MRO/MCS declared the storm system to be a planet encircling dust event (PEDE). By 8 June (Ls ~189) the PEDE was detectable in the upper atmosphere by multiple orbiting spacecraft including MRO (Wolkenberg et al.,2020, Kass et al.,2020, Elrod et al.,2020, Jain et al.,2020, Rao et al., 2020 etc.). The PEDE peaked by 7-13 July (Ls ~207-210) as determined by zonally averaged temperatures observed by MRO/MCS in the middle atmosphere (Kass et al., 2020). The PEDE maximum correlates with the highest optical depth and largest increase in

69 densities and scale heights in the upper atmosphere as measured by Mars Atmosphere and
70 Volatiles EvolutioN (MAVEN) Neutral Gas and Ion Mass Spectrometer (NGIMS) (Elrod et
71 al.,2020). The dust storm lasted for a little over a month with the decay occurring around mid-
72 September allowing the atmosphere to show signs of returning to seasonal and diurnal normal
73 (Ls ~180 - 240).

74 Helium, a light element, has a large scale height (H) in the upper atmosphere like
75 hydrogen, but it has the uniqueness of being non-reactive, so it is not influenced by chemistry
76 with carbon and oxygen in the atmosphere. This allows He to become a tracer for the
77 atmospheric circulation. Being much lighter than the bulk of the atmosphere, He will pool in the
78 colder, condensed, parts of the atmosphere, typically the winter polar dawn region near
79 solstices and equinoxes at mid-to- high latitudes. This light species transport occurs by the
80 process of wind-induced diffusion (e.g., Mayr et al. 1978; 1980) that operates on Earth and
81 Venus as well. Previous studies of the He in the upper atmosphere of Mars have shown an
82 agreement with this behavior (Elrod et al., 2017; Gupta et al., 2021). Mars Year 34 was an
83 exception. While MAVEN was in a good position to be able to observe the winter polar dawn
84 side He bulge, there was no He bulge observed. This sampling period was different because MY
85 34 encountered a Planet Encircling Dust Event (PEDE). Studies are emerging that the dynamics,
86 heating, composition, and chemistry in the upper atmosphere were all modified during the
87 global dust storm (e.g., Elrod et al., 2020; Stone et al., 2020, Jain et al., 2020).

88 The impact of the global dust storm has been shown to have an increase in water ice at
89 higher altitudes than previously measured (Stone et al., 2020) along with compositional
90 changes to the upper atmosphere (Elrod et al., 2020; Farahat et al., 2021). The compositional

changes in the upper atmosphere indicated that the lighter species, specifically the O and N_2 were reduced during the PEDE compared to the main species (CO_2 and Ar). Additional examination of the nightside and dusk data taken by NGIMS during the PEDE also revealed that the He density was lower than expected for the predicted He bulge.

Mars has a He bulge (Elrod et al., 2017) that peaks in density where the temperatures of the upper atmosphere are relatively cool. MAVEN/NGIMS has obtained in-situ observations of He for 5 Mars Years (MY), MY32 – 36. He density peaks are highest around equinox (Ls ~0, or 180) near mid to high latitudes (lat ~45-70^o) and winter solstice (Ls ~90 or 270) near corresponding high latitudes (lat ~55-80) on the night or dawn side local solar time (LST) of ~22-5 h. Due to the eccentricity of the Martian orbit, there is some observed asymmetry between the northern and southern He bulge (Gupta et al., 2021).

We selected data from MAVEN/NGIMS from MY 32, 34 and 35. These three MY's were chosen because NGIMS is an in-situ instrument and to detect the He the spacecraft needs to be passing through the desired region and approximate local time. During MY 32, 34 and 35 MAVEN was in the northern hemisphere from Ls ~180-280 and on the dawn through night-side (~20 h – 6h LST) for each of these years.

Helium data from Martian years during which dust storms are only small regional storms (constrained to just the southern hemisphere or are short lived) were compared to the MY 34 global dust storm event. The He densities were found to be substantially lower during the global dust event where the bulge should have been observed. Mars Global Ionosphere Thermosphere Model (M-GITM) (Bougher et al. 2015) numerical model simulations demonstrated that under normal circumstances during northern winter (Ls ~180-240) a He

bulge should form in the upper latitudes (lat ~50-70^{o}) and night to dawn sectors (LST ~20-6h) (Elrod et al., 2017). MAVEN NGIMS began observations during the PEDE at mid-latitudes and on the dawn-side at mid to low latitudes (~20^{o} – 35^{o}) moving to dusk/night (LST ~15-3h; lat 35-65^{o}). While not the most ideal observation for the He bulge detection, this still should have been sufficient to observe a bulge similar to what was observed in other comparable years like MY 32 &35.

2. Methods

2.1 Dataset Collection

MAVEN has an inclined orbit with a periapsis of ~150 km from 2014-2020; this periapsis was then raised to ~180-200 km after Aug 2020 (mid MY 35). NGIMS is an in-situ mass spectrometer that takes measurements of the upper atmosphere during periapsis from below ~500 km (Mahaffy et al., 2015). These orbits and measurements allow NGIMS to vary observation between all local times and latitudes throughout the Martian year. Due to the limit of observations, and the fact that dust storm season typically occurs around Ls ~180-290, we needed to select data from the northern hemisphere, latitudes >45^{o} and preferably also after 18h and before 6h local solar time (LST). MAVEN/NGIMS had this orientation during MY 32, 34 and 35. In MY 33 the spacecraft was in the southern hemisphere for Ls ~200-360 and unable to observe the He bulge.

While the higher altitudes have not been ideal for study of the Martian upper atmosphere, NGIMS has continued to conduct regular science. The higher altitude measurements had an impact on the heavier species (CO_2, Ar and O) measurements, but since He is a light element and has a large-scale height (nearly vertical density variation), the higher

altitude measurements had little impact. Due to its large scale height, the He densities measured between 175km and 220km are very similar in the thermosphere. For this reason, we used data from 170km – 225km from MY 32, 34 and 35 for coverage and for better statistics. Since the PEDE began at Ls ~180 and extended through Ls ~240, and since the He bulge should be forming in the northern polar region as this is near northern winter, we restricted our data to this range and latitude 0-70^{o}N.

2.2 Modeling

The Mars Global Ionosphere-Thermosphere Model (M-GITM) is a model framework essentially combining the terrestrial GITM framework (e.g., Ridley et al., 2006) with Mars fundamental physical parameters, ion-neutral chemistry, and key radiative processes in order to capture the basic observed features of the thermal, compositional, and dynamical structure of the Mars atmosphere from the ground to ~250 km (e.g., Bougher et al., 2015). The model has 5^{o} horizontal resolution and 2.5 km vertical resolution.

The modern M-GITM code currently simulates the conditions of the Martian atmosphere near the traditional exobase all the way to the surface (Bougher et al., 2015). For the Mars lower atmosphere (0-80 km), a state-of-the-art correlated-k radiation code was adapted from the NASA Ames Mars General Circulation Model (MGCM) (Haberle et al., 2003) for incorporation into M-GITM. This provides solar heating (long and short wavelength), seasonally variable aerosol heating, and CO_2 15-micron cooling in the local thermal equilibrium (LTE) region of the Mars atmosphere (below ~80 km). For the Mars upper atmosphere (~80-250 km), a modern CO_2 non-local thermal equilibrium (NLTE) 15-µm cooling scheme has

156 recently been implemented (e.g., Gonzalez-Galindo et al., 2013), along with MAVEN Extreme
157 ultra-violet monitor (EUVM) L3 solar fluxes taken from the Flare Irradiance Spectrum Model
158 (Mars) (FISM-M) empirical model outputs on a daily cadence (Thiemann et al., 2017). M-GITM
159 thermospheric heating, dissociation and ionization rates are all simulated at each model time
160 step (e.g., Bougher et al., 2015).

161 Recently, an existing non-orographic, whole atmosphere gravity wave (GW) momentum
162 and energy deposition scheme (e.g., Yigit et al., 2008; Medvedev et al. 2015) has been
163 incorporated within the M-GITM code in order to examine the impacts of GWs upon the
164 thermospheric wind, density, and temperature structure (see Roeten et al., 2022b). Adding
165 schemes to parameterize unresolved physical phenomena, such as GWs, is a common approach
166 for relatively low-resolution global models like M-GITM. Under typical (non-dust storm)
167 conditions, it has been previously reported that with the addition of this GW scheme into M-
168 GITM, simulated global winds can be reduced by a factor of two, and temperatures are
169 generally cooled at all latitudes at thermosphere heights, but especially at high latitudes (see
170 Roeten et al. 2022a,b), compared to simulations without the scheme. Since the addition of GW
171 effects into M-GITM was found to produce large impacts on the modeled general circulation, a
172 M-GITM simulation during the PEDE which utilizes the GW scheme was also examined here to
173 see if there was any apparent difference in the He distribution. For the M-GTIM simulations in
174 the current analysis which utilize the GW scheme, the adjustable parameters (e.g., horizontal
175 wavelength, source momentum flux) are set to the same values used in the standard GW
176 simulations of Roeten et al. (2022b).

3. Data Analysis and Results

3.1 Analysis

Figure 1a compares the data for all three years and 1b plots the latitude and local solar time sampling of NGIMS from MY 32-36. The scattered density data is for each orbit while the solid lines are 10-orbit averages. MY 32 is in grey diamonds (with yellow line average), MY 34 is in red stars (with blue line average) and MY 35 is in black triangles (with cyan line average). All three years show seasonal He bulges throughout the Mars Year. This paper is focused on the He bulges that form during the northern winter polar region from Ls ~180 – 270. The peaks and troughs matched as modeled by M-GITM seasonally between MY 32, 34, and 35, with the singular exception of MY 34 around Ls ~180 – 240 during the dust event.

We focused on the PEDE time frame from Ls ~180-280 in figure 2 and created a 10-orbit average to clarify the inter-annual data comparisons. MY 32 is in light grey diamonds, MY 35 is in dark grey triangles and MY 34 is in red stars in the density panel (a). Panel (b) is the temperature data in which the light grey diamonds are MY 32, red squares MY 34, and black triangles are MY 35. There is a distinctly different pattern in the densities for MY 34 during the PEDE (Ls ~240-260), for which the He density is lower where there is a measured increase observed in MY 32 and 35 due to the typical He bulge. In addition, the MY 34 temperatures are higher on the night and dawn side compared to the other MY's at the same latitude and LST. The higher MY 35 temperatures are from the lower latitudes and dayside. All densities are from the inbound portion of the orbit segment and are measured at ~200km altitude.

Figure 3 shows the M-GITM modeling of the He bulge from Ls ~180 - 240 near the time of the PEDE in MY 34. The top panel is the predicted He from Ls ~180- 240, approximately the time of the PEDE including the dust levels as observed by MRO/MCS (Kass et al., 2020). It does nominally agree with previous M-GITM modeling without the PEDE dust levels used to compare with the MY 32 and 35 data (Rao et al., 2020; Elrod et al., 2017). The bottom panel is the updated revision of the M-GITM model implementing both the gravity wave parameterization scheme and dust conditions anticipated from Ls ~180-240 during the PEDE. The M-GITM model without gravity waves, as compared with the data from MY32 and MY 35 was found to be a good match to the data, as shown in Gupta et al., (2021) and Elrod et al., (2017) especially for the high latitudes. However, Gupta et al, (2021), and Fig 2 show that the MY 34 data is not the same and that the match with the M-GITM model is not the same as MY 32 and 35. The NGIMS data indicate a substantial change in the He distribution in the northern hemisphere during the northern winter season. When comparing the M-GITM model simulations which used nominal dust conditions related to the PEDE but did not incorporate the effects of gravity waves with the NGIMS data, the results did not match particularly well as compared with other Mars Years especially in the high latitudes and near midnight. Because of this disagreement with the M-GITM model with dust but without gravity waves, we determined to revise the computation and incorporate gravity waves. The revised M-GITM model NGIMS MY 34 He density data comparison (fig 4) that included gravity waves, improved the comparison on the dawn side, but there continues to be a mismatch between the data and model at the high latitudes (~50^{o}N latitude) and near midnight (discussed further in section 3.2).

We examined the impacts on the global circulation by conducting M-GITM simulations for MY 34 during the PEDE from its onset at Ls ~184 to its peak (Ls ~208—210) and through the decay phase (Ls ~240). We compared this with the observed NGIMS data available through the period. A first M-GITM simulation is run for solar forcing, a globally uniform eddy diffusion prescription, and an evolving dust distribution that matches MRO/MCS dust measurements during the evolution of the PEDE. The M-GITM computed He bulge is larger than expected near the dawn region above ~50^{o}N latitude. The simulated He bulge after midnight is also too large, with a much bigger difference to the data results. In short, M-GITM meridional appear to be too strong in this vicinity.

A second M-GITM simulation is run with the addition of the new non-orographic gravity wave momentum and energy deposition scheme previously described (Roeten et al., 2022b). Standard gravity wave parameters are used that are proven to be robust, but have not included any changes with season, or disruption that may have occurred specifically with this dust event. The major impact is to slow winds (both zonal and meridional) and cool high latitude temperatures especially. The computed He bulge is shown to move further northward (poleward of 50^{o}N at the dawn terminator), providing a reduction in magnitude that reasonably matched available NGIMS measurement as shown in figures 3 and 4. However, the mismatch with the post-midnight bulge indicated the simulated bulge is still much larger than the NIGMS measurements.

We do acknowledge that gravity waves could be evolving (i.e., non-constant) throughout the PEDE storm (Yiğit et al., 2021), yet our current GW modeling is presently limited

to unchanging gravity wave parameters. We plan to make this revision in future efforts to determine how variable gravity waves are impacting the He bulge during the PEDE.

3.2 Results

Figure 4 (panels a and b) compare the NGIMS density data with the M-GITM prediction. The M-GITM output are binned by the NGIMS trajectory through the dust event (Ls ~180-240). Figure 4 plots the M-GITM density data that is binned with the NGIMS density data. The $\log_{10}$ of the density was then taken and the difference between the model (M-GITM) and the data (NGIMS) was computed. Panel (a) plots the difference of the model with the use of the gravity wave scheme and panel b the model without gravity waves. The scales between panel (a) and (b) are not equal. The match between model and data is much better for the case where gravity wave effects are included in the model (panel a) than the for the case where the gravity wave scheme is not included in the model (panel b). However, the biggest differences occur once the measurements are examined around midnight and ~50^{o}N latitude. The model indicates there should be a substantial observed He bulge both on the dawn side and after midnight above 50^{o}N latitude. However, the NGIMS data above 50^{o}N lat, from midnight to 22h does not substantially increase, unlike the M-GITM model, where the He bulge is predicted to be redistributed around the northern pole (figure 2), this is where the model and data disagree. The discrepancy is likely due to the atmospheric dynamics owing to changes in the gravity waves, eddy diffusion rates, and circulation, during the dust storm which needs to be better addressed within the M-GITM model (see section 4).

The densities in the computed M-GITM model which include gravity wave effects match the NGIMS density data much better on the dawn side (LST ~1-5h) and in the mid to high latitudes (~0-50^{o}N lat). But once the spacecraft move closer to midnight and above 50^{o}N the mismatch between the model and data become much greater. This was also where the model predicted the presence of the He bulge should be able to be observed. NGIMS did not observe a significant increase in the He data above 50^{o}N latitude on the nightside around midnight (LST ~1-22h).

Figure 5 compares the M-GITM modeled temperatures with the NGIMS measured temperatures during the dust event. Again, the M-GITM model data has been binned to correspond with the NGIMS data, and the M-GITM temperatures have been subtracted from the NGIMS temperatures. Panel A is the difference for the measured NGIMS temperature data and the model simulations which includes the GW scheme and panel B is the model simulations which did not use the GW scheme. In both cases the scales are the same, and the M-GITM model temperatures are consistently cooler than the NGIMS measured temperatures. The temperatures do match better for the gravity wave case than for the non-gravity wave case, which indicates that the model upgrade employing gravity waves is a good improvement to the model.

4. Discussion

The reduced He bulge density during the PEDE in 2018 may indicate that the upper atmosphere was more turbulent (i.e., on the night and dawn side) than other recent MY. While NGIMS wind measurements were obtained at the beginning and during the dust storm, the campaign averaged wind speeds were not significantly different from those measured in

campaigns prior to or after the PEDE (Roeten et al., 2022a)). While substantial winds are present throughout the dust storm in the upper atmosphere, large variations of these winds from orbit-to-orbit were also observed, possibly connected to increased gravity wave activity which was also observed in the thermosphere at the same time (Yiğit et al., 2021)

NGIMS neutral data has been used to catalog gravity wave observations both on the dayside and night-side during non-dust seasons (England et al., 2017). Yiğit et al (2021) conducted an analysis of the gravity wave activity seen in the upper atmosphere during the PEDE by analyzing perturbations induced in the NGIMS CO2 densities and found that thermospheric gravity wave activity doubles during the peak of the dust storm. In addition to gravity waves causing short time-scale variability, the momentum deposited by gravity waves also modifies the middle-upper atmospheric circulation, as seen in several Global Circulation Model (GCM) studies (e.g., Medvedev et al., 2012, 2013; Kuroda et al., 2020). A modeling study examining the full impact of variations in the gravity waves on the atmospheric circulation or the He bulge has not yet been completed.

The He bulge forms in the cool parts of the atmosphere. Therefore, the highest levels of He are found from ~0-5h LST at high latitudes during the winter solstice, and at mid to high latitudes from ~0-5h LST during the equinox (Gupta et al., 2021, Elrod et al., 2017). The fact that in MY 34 during the dust event this He bulge did not appear from 0-5h in the high latitudes indicates a change in the circulation of the upper atmosphere or that the dawn side sector was much warmer than predictions. The temperature differences shown in figure 5 match better for the M-GITM non-gravity wave case in the higher latitudes (above ~50^{o} N lat) but the case in which the gravity wave scheme was included in the model matches a little better for the mid

latitudes. In both cases, however, the model temperatures are too cool compared to the observed NGIMS temperatures. This could help to provide possible insight for needed changes to the gravity wave parameters used in the model. It could also lead to a new avenue of investigation on the eddy diffusion coefficient.

Alternatively, it is possible and even likely that NGIMS sampling passed just south of the polar He bulge and never observed the redistributed He due to the PEDE. One possibility is that NGIMS missed the He bulger that was redistributed as the M-GITM model predicted during the PEDE. Specifically, NGIMS did not pass above ~50^0N lat until almost Ls ~224, which was past the peak of the dust storm. It is possible that the He bulge, and upper atmosphere circulation was no longer distributed around the pole but moved away from the night side and more to the dawn side as the dust storm dissipated much faster than our current model predicts.

5. Summary

The He density is a tracer of the Martian upper atmosphere circulation. The He bulge was reduced in MY 34 as compared to MY 32 and MY 35 at similar latitudes and LST, i.e., above 50^oN latitude for night and dawn observations. Similar observations during MY 32 and 35 during non-dust storm years clearly observed He bulges during similar conditions. The lack of He bulge in MY 34 due to the PEDE may indicate changes in the global thermospheric circulation.

Our conclusion thus far is that the gravity wave scheme we have employed in the M-GITM model is a significant improvement for driving more realistic Mars thermospheric circulation (Roeten et al., 2022b). As a result, an improved picture is emerging describing how He is moving in the upper atmosphere and how the thermospheric circulation is changing

during the PEDE. Gravity waves may be reducing the strength of the global thermospheric circulation and thereby improving the dawn region He bulge distribution and magnitude soon after the peak of the PEDE. However, a refined gravity wave scheme may be needed that accounts for the time evolution of GW parameters and the resulting momentum/energy deposition impacting the circulation from the PEDE peak through the decay phase. The presently computed He bulge magnitude is too large (especially above 50^{o}N latitude around midnight) and does not match the NGIMS observed values.

Additionally, we suspect that changes in the small-scale eddy diffusion could be playing a role in modifying the global circulation during the PEDE that are not accounted for. For example, the small-scale eddy diffusion (within the high latitude winter polar dawn and night regions) may be enhanced during this time due to the heating of the dawn and night side from the dust storm, short-circuiting the impact of global circulations, thereby reducing the magnitude of the high latitude winter polar Helium bulge. Further studies and modeling are required to determine this effect.

The data-model discrepancies may also be due to the combined effects of M-GITM gravity wave parameters plus eddy diffusion coefficients that thus far do not change with season, or with respect to the dust event. Specifically, the atmospheric height where gravity waves are launched probably does changes with season, and the corresponding source momentum flux may evolve during the PEDE as well (e.g., Yiğit et al., 2021). Alternatively, missing physics may be important to include. This immediately points to the need to expand the non-orographic gravity wave scheme to incorporate the self-consistent calculation of the eddy diffusion. In particular this may yield an effective eddy diffusion coefficient that varied

with global location (e.g. winter polar night) and background atmospheric conditions during the PEDE. Helium and other light species continue to be an important marker for the upper atmosphere in terms of escape and changes with the global circulation.

Limitations with NGIMS observations, given that it is the only in-situ upper atmosphere instrument currently delivering He density, is one other factor to be considered in the distribution of the He bulge. While other Mars orbiters like Mars Orbiter Mission which has a similar instrument to NGIMS were also observing the PEDE (Rao et al., 2020), it is unfortunately very limited in the light species observations (Bardwaj et al., 2016).

6. Acknowledgements

This work is supported by the MAVEN spacecraft mission. The material is based upon work supported by NASA under award number 80GSFC21M0002.

7. Data Acknowledgement Statement

All MAVEN NGIMS data used in this work is publicly available on the Planetary Data System (PDS) (Benna and Lyness, 2014).

In addition, solar fluxes used for M-GITM model simulations are taken from the MAVEN/EUVM FISM-M empirical model corresponding to a Level 3 Version 14, Revision 3 data product on the PDS (Eparvier, 2022).

Finally, the MGITM data is publicly available on the University of Michigan Deep Blue Data repository (e.g. Roeten and Bougher, 2022).

8. References

Bhardwaj, A., Thampi, S. V., Das, T. P., Dhanya, M. B., Naik, N., Vajja, D. P., Pradeepkumar, P., Sreelatha, P., Supriya, G., K., A. J., et al. (2016), On the evening time exosphere of Mars: Result from MENCA aboard Mars Orbiter Mission, *Geophys. Res. Lett.*, 43, 1862– 1867, doi:10.1002/2016GL067707.

Benna, M., & Lyness, E. (2014). MAVEN Neutral Gas and Ion Mass Spectrometer [Dataset], NASA Planetary Data System. doi: https://doi.org/10.17189/1518931

Bougher, S. W., Pawlowski, D., Bell, J. M., Nelli, S., McDunn, T., Murphy, J. R., Chizek, M., and Ridley, A. (2015), Mars Global Ionosphere-Thermosphere Model: Solar cycle, seasonal, and diurnal variations of the Mars upper atmosphere. *J. Geophys. Res. Planets*, 120, 311–342. doi: 10.1002/2014JE004715.

Elrod, M. K., Bougher, S., Bell, J., Mahaffy, P. R., Benna, M., Stone, S., Yelle, R., and Jakosky, B. (2017), He bulge revealed: He and CO_2 diurnal and seasonal variations in the upper atmosphere of Mars as detected by MAVEN NGIMS, *J. Geophys. Res. Space Physics*, 122, 2564– 2573, doi:10.1002/2016JA023482.

Elrod, M. K., Bougher, S. W., Roeten, K., Sharrar, R., & Murphy, J. (2020). Structural and Compositional Changes in the Upper Atmosphere Related to the PEDE-2018 Dust Event on Mars as Observed by MAVEN NGIMS. *Geophysical Research Letters*, 47, e2019GL084378. https://doi.org/10.1029/2019GL084378

England, S. L., Liu, G., Yiğit, E., Mahaffy, P. R., Elrod, M., Benna, M., Nakagawa, H., Terada, N., and Jakosky, B. (2017), MAVEN NGIMS observations of atmospheric gravity waves in the Martian thermosphere, *J. Geophys. Res. Space Physics*, 122, 2310– 2335, doi:10.1002/2016JA023475.

Eparvier, F. G. (2022). MAVEN EUV Modeled Data Bundle [Dataset], NASA Planetary Data System. doi: doi.org/10.17189/1517691

Farahat, A., Mayyasi, M., Withers, P., Dayeh, M. A., & Abuelgasim, A. (2021). Effects of the June 2018 global dust storm on the atmospheric composition of the Martian upper atmosphere as observed by MAVEN. *Journal of Geophysical Research: Planets*, 126, e2021JE006868. https://doi.org/10.1029/2021JE006868

Felici, M., Withers, P., Smith, M. D., González-Galindo, F., Oudrhiri, K., & Kahan, D. (2020). MAVEN ROSE observations of the response of the Martian ionosphere to dust storms. *Journal of Geophysical Research: Space Physics*, 125, e2019JA027083. https://doi.org/10.1029/2019JA027083

González-Galindo, F., Chaufray, J.-Y., López-Valverde, M. A., Gilli, G., Forget, F., Leblanc, F., Modolo, R., Hess, S., and Yagi, M. (2013), Three-dimensional Martian ionosphere model: I. The photochemical ionosphere below 180 km, *J. Geophys. Res. Planets*, 118, 2105-2123, doi:10.1002/jgre.20150.

Gupta, N., Rao, N. V., Bougher, S., & Elrod, M. K. (2021). Latitudinal and seasonal asymmetries of the helium bulge in the Martian upper atmosphere. *Journal of Geophysical Research: Planets*, 126, e2021JE006976. https://doi.org/10.1029/2021JE006976

Haberle, Robert M., Murphy, James R., Schaeffer, James, (2003) Orbital change experiments with a Mars general circulation model. *Icarus,* Volume 161, Issue 1, Pages 66-89, ISSN 0019-1035, https://doi.org/10.1016/S0019-1035(02)00017-9.

Heavens, N. G., Kass, D. M., & Shirley, J. H. (2019). Dusty deep convection in the Mars Year 34 planet-encircling dust event. *Journal of Geophysical Research: Planets*, 124, 2863–2892. https://doi.org/10.1029/2019JE006110

Jain, S. K., Bougher, S. W., Deighan, J., Schneider, N. M., Gonzalez-Galindo, F., Stewart, A. I. F., et al. (2020). Martian thermospheric warming associated with the Planet Encircling Dust Event of 2018. *Geophysical Research Letters*, 47, e2019GL085302. https://doi.org/10.1029/2019GL085302

Kass, D. M., Schofield, J. T., Kleinböhl, A., McCleese, D. J., Heavens, N. G., Shirley, J. H., & Steele, L. J. (2020). Mars Climate Sounder observation of Mars' 2018 global dust storm. *Geophysical Research Letters*, 47, e2019GL083931. https://doi.org/10.1029/2019GL083931

Kuroda, T., Medvedev, A. S., & Yiğit, E. (2020). Gravity wave activity in the atmosphere of Mars during the 2018 global dust storm: Simulations with a high-resolution model. *Journal of Geophysical Research: Planets*, 125 e2020JE006556. https://doi.org/10.1029/2020JE006556

Leelavathi, V., Venkateswara Rao, N., & Rao, S. V. B. (2020). Interannual variability of atmospheric gravity waves in the martian thermosphere: Effects of the 2018 planet-encircling dust event. *Journal of Geophysical Research: Planets*, 125, e2020JE006649. https://doi.org/10.1029/2020JE006649

Mahaffy, P. R., Benna, M., Elrod, M., Yelle, R. V., Bougher, S. W., Stone, S. W., and Jakosky, B. M. (2015), Structure and composition of the neutral upper atmosphere of Mars from the MAVEN NGIMS investigation, *Geophys. Res. Lett.*, 42, 8951– 8957, doi:10.1002/2015GL065329.

Mayr, H. G., Harris, I., Hartle, R. E., and Hoegy, W. R. (1978), Diffusion model for the upper atmosphere of Venus, *J. Geophys. Res.*, 83(A9), 4411– 4416, doi:10.1029/JA083iA09p04411.

Mayr, H. G., Harris, I., Niemann, H. B., Brinton, H. C., Spencer, N. W., Taylor, H. A., Hartle, R. E., Hoegy, W. R., and Hunten, D. M. (1980), Dynamic properties of the thermosphere inferred from Pioneer Venus Mass Spectrometer measurements, *J. Geophys. Res.*, 85(A13), 7841– 7847, doi:10.1029/JA085iA13p07841.

Medvedev, A. S., and Yiğit, E. (2012), Thermal effects of internal gravity waves in the Martian upper atmosphere, *Geophys. Res. Lett.*, 39, L05201, doi:10.1029/2012GL050852.

Medvedev, A. S., Yiğit, E., Kuroda, T., and Hartogh, P. (2013), General circulation modeling of the Martian upper atmosphere during global dust storms, *J. Geophys. Res. Planets*, 118, 2234-2246, doi:10.1002/2013JE004429.

Miyamoto, A., Nakagawa, H., Kuroda, T., Takami, K., Murata, I., Medvedev, A. S., et al. (2021). Intense zonal wind in the Martian mesosphere during the 2018 planet-encircling dust event observed by ground-based infrared heterodyne spectroscopy. *Geophysical Research Letters*, 48, e2021GL092413. https://doi.org/10.1029/2021GL092413

Rao, Venkateswara, N., Gupta, N., & Kadhane, U. R. (2020). Enhanced densities in the Martian thermosphere associated with the 2018 planet-encircling dust event: Results from MENCA/MOM and NGIMS/MAVEN. *Journal of Geophysical Research: Planets*, 125, e2020JE006430. https://doi.org/10.1029/2020JE006430

Roeten, K. J., & Bougher, S. W. (2022c). M-GITM datasets used for a modeling study of the mean impacts of subgrid-scale gravity waves on thermospheric velocities and temperatures at Mars [Dataset]. University of Michigan - Deep Blue Data. doi.org/10.7302/7hab-2340

Roeten, K. J., Bougher, S. W., Benna, M., Mahaffy, P. R., Lee, Y., Pawlowski, D., et al. (2019). MAVEN/NGIMS thermospheric neutral wind observations: Interpretation using the M-GITM general circulation model. *Journal of Geophysical Research: Planets*, 124, 3283– 3303. https://doi.org/10.1029/2019JE005957

Roeten, K.J., S.W.Bougher, M.Benna, M.K.Elrod (2022a), MAVEN/NGIMS wind observations in the martian thermosphere during the 2018 planet encircling dust event. *Icarus*, *vol 382, https://doi.org/10.1016/j.icarus.2022.115006*

Roeten, K. J., Bougher, S. W., Yiğit, E., Medvedev, A. S., Benna, M., & Elrod, M. K. (2022b). Impacts of gravity waves in the Martian thermosphere: The Mars Global Ionosphere-Thermosphere Model coupled with a whole atmosphere gravity wave scheme. Journal of Geophysical Research: Planets, 127, e2022JE007477. https://doi.org/10.1029/2022JE007477

Ridley, A.Ja., Deng, Y., Tóth, G., (2006) The global ionosphere–thermosphere model. *Journal of Atmospheric and Solar-Terrestrial Physics*,Volume 68, Issue 8, Pages 839-864, https://doi.org/10.1016/j.jastp.2006.01.008

Stone, S. W., Yelle, R. V., Benna, M., Elrod, M. K., & Mahaffy, P. R. (2022). Neutral composition and horizontal variations of the Martian upper atmosphere from MAVEN NGIMS. *Journal of Geophysical Research: Planets*, 127, e2021JE007085. https://doi.org/10.1029/2021JE007085

Stone, S. W., Yelle, R. V., Benna, M., Elrod, M. K., & Mahaffy, P. R. (2018). Thermal structure of the Martian upper atmosphere from MAVEN NGIMS. *Journal of Geophysical Research: Planets*, 123, 2842– 2867. https://doi.org/10.1029/2018JE005559

Stone, Shane W., Yelle, Roger V., Benna, Mehdi, Lo, Daniel Y., Elrod, Meredith K., Mahaffy, Paul R., (2020) Hydrogen escape from Mars is driven by seasonal and dust storm transport of water. *Science vol. 370 No 6518* https://doi.org/10.1126/science.aba5229

Thiemann, E., Chamberlin, P. C., Eparvier, F., Woods, T., Bougher, S. W., Jakosky, B. M, and Templeman, B. (2017), The MAVEN EUVM spectral irradiance model for solar variability at Mars: Algorithms and results, J. Geophys. Res. Space Physics, 122, 2748-2767. doi:10.1002/2016JA023512

Wolkenberg, P., Giuranna, M., Smith, M. D., Grassi, D., & Amoroso, M. (2020). Similarities and differences of global dust storms in MY 25, 28, and 34. *Journal of Geophysical Research: Planets*, 125, e2019JE006104. https://doi.org/10.1029/2019JE006104

Yiğit, E., Medvedev, A. S., Benna, M., & Jakosky, B. M. (2021). Dust storm-enhanced gravity wave activity in the Martian thermosphere observed by MAVEN and implication for atmospheric escape. *Geophysical Research Letters*, 48, e2020GL092095. https://doi.org/10.1029/2020GL092095

Figure 1

(a)

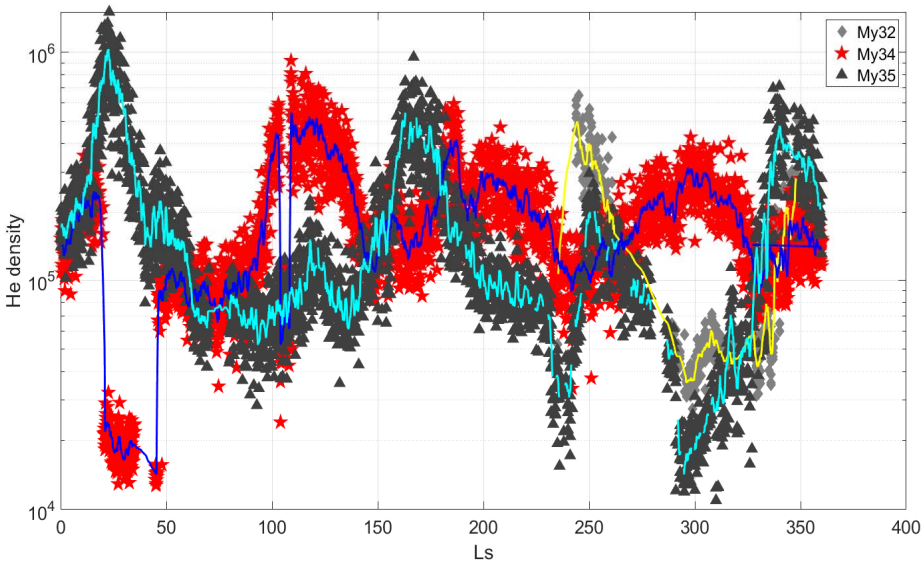

(b)

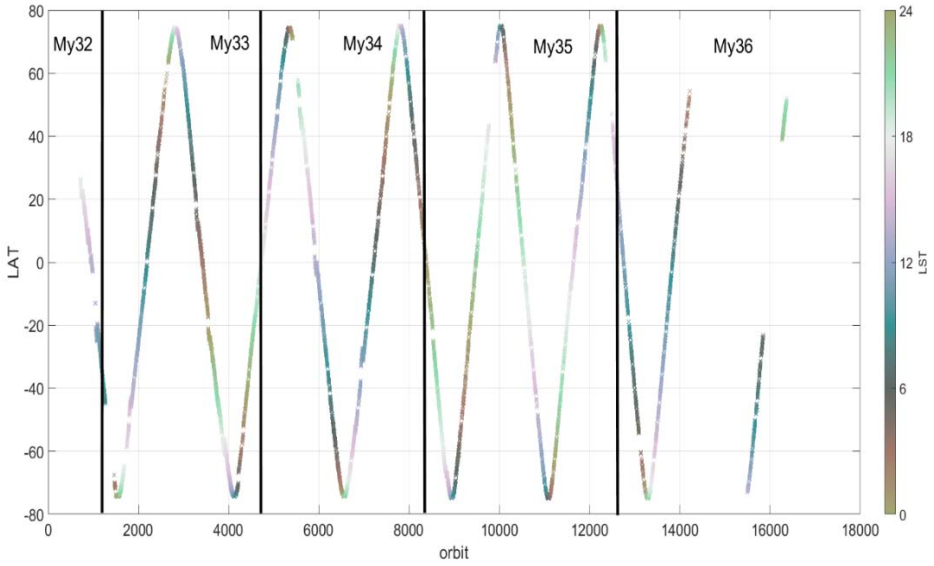

Figure 1 (a) Helium (He) density data from MY 32 (grey diamonds), MY 34 (red stars) and MY 35 (black triangles). The solid lines mark the 10-orbit average for each of these years. The He peaks correspond with the instrument passing through the seasonal He bulges in the upper latitudes on the dawn to night side in the thermosphere. (b) The latitude vs orbit and local solar time

499 (LST) of NGIMS throughout the mission. The color bar indicate the LST. In MY 32, 34, and 35,
500 NGIMS was in the northern hemisphere and dawn and/or night side between Ls ~180-240. In
501 MY 33 and 36 NGIMS was in the wrong hemisphere or the data was unavailable.
502

503 Figure 2

504 (a)

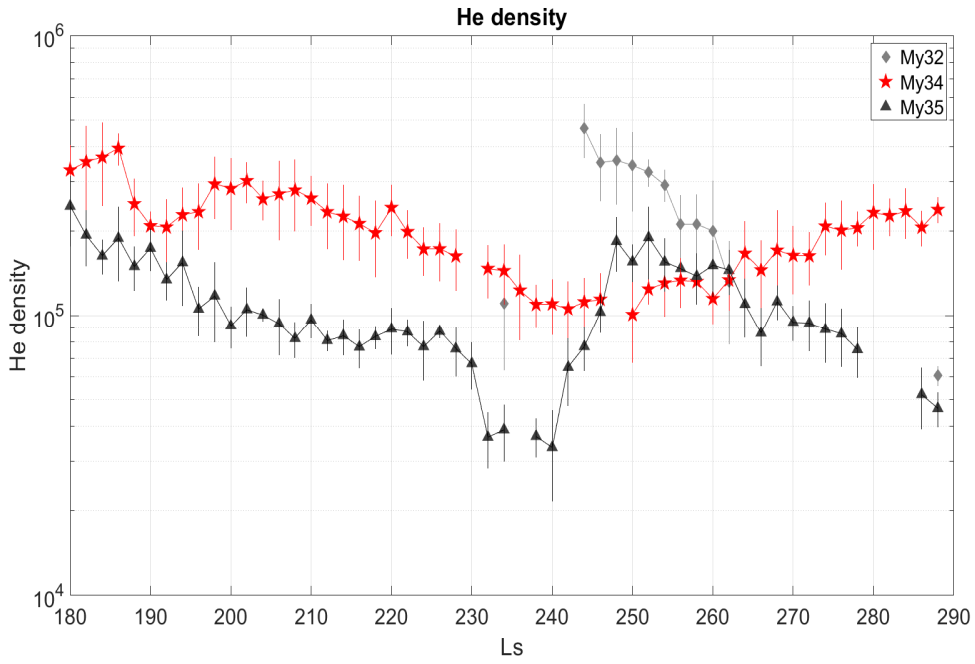

505

506 (b)

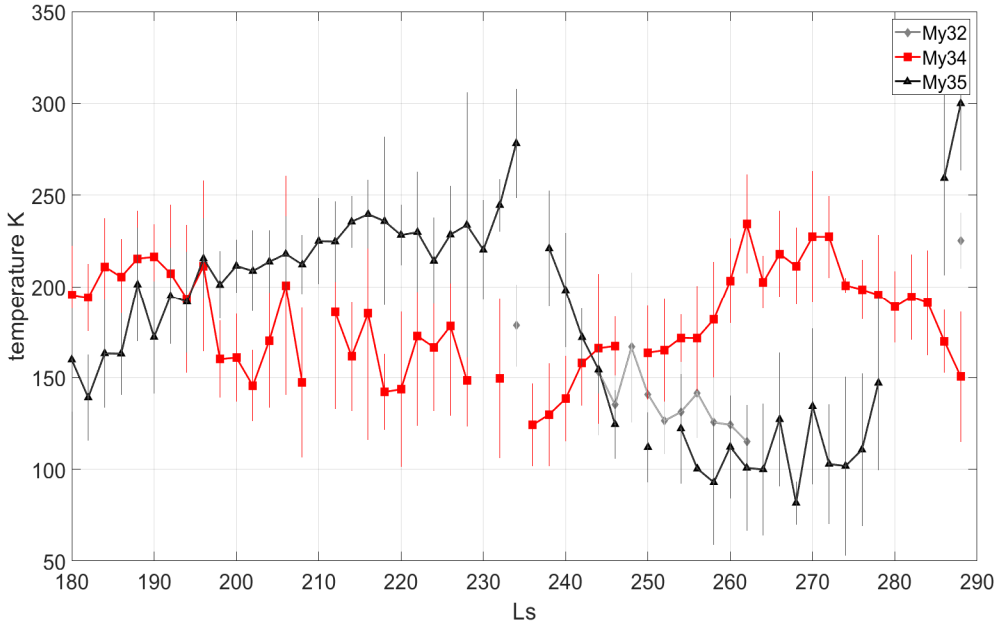

507

508 Figure 2 (a) Ten orbit averaged Helium density from Ls ~180-280 for MY32 (grey diamonds),
509 MY34 (red squares) and MY35 (black triangles). He density clearly increases for MY 32 &35 as
510 predicted for observation of He bulge during northern polar winter solstice. (b) Temperatures
511 from MY32 (light grey diamonds), MY 34 (red squares), and MY 35 (black triangles) from Ls
512 ~180-280. The temperatures from MY 34 are higher in high latitudes and night side than during
513 the other three years at the same conditions. (Note the high temperatures here during MY 35
514 are day side, mid latitude)
515

516 Figure 3

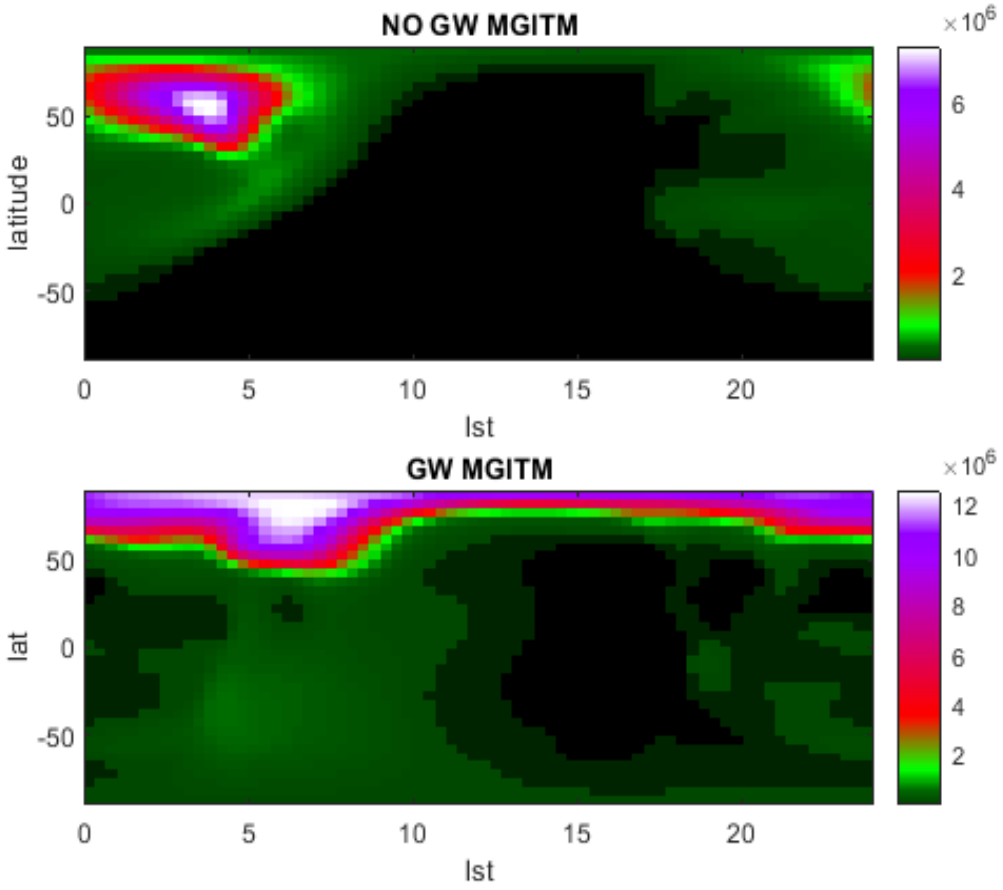

517

518 Figure 3 M-GITM computed He densities. Top panel are the computed densities from the model
519 without employing gravity waves. The bottom panel is revised with gravity waves. Both models
520 are from Ls ~180-240 and account for increased dust in the thermosphere during the dust
521 event.
522

523
524 Figure 4

525 (a)

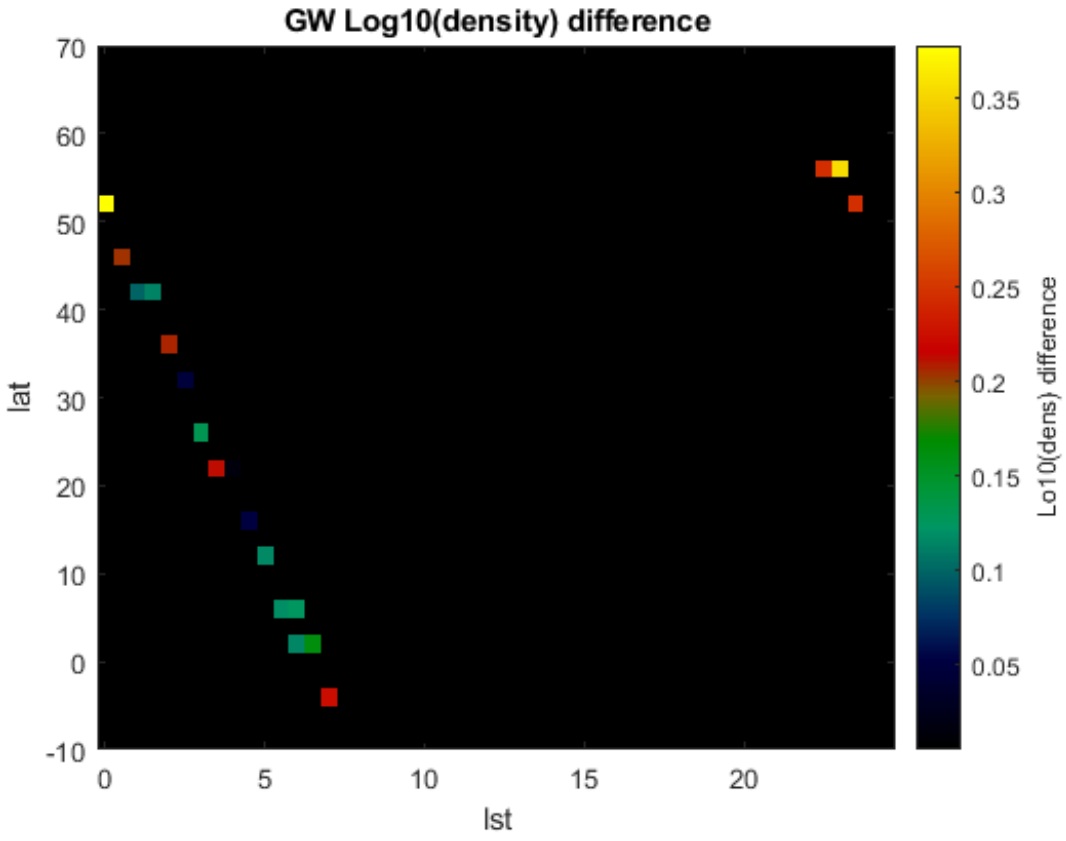

526

527 (b)

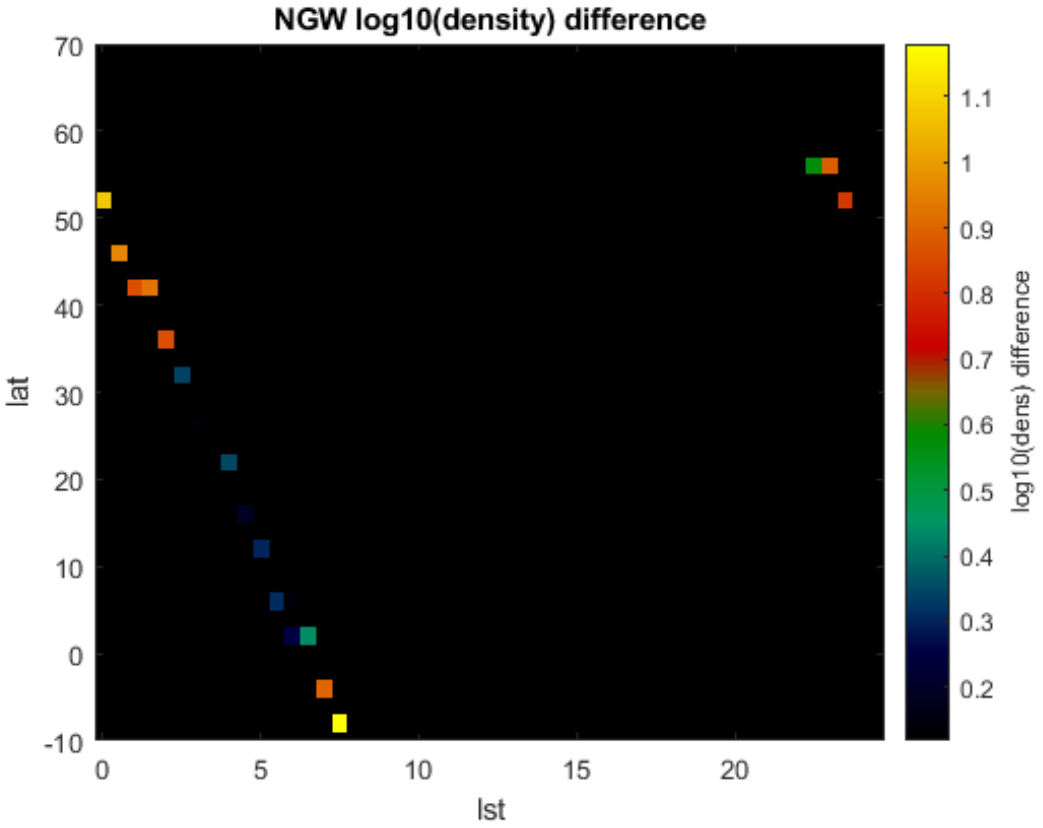

528

529 Figure 4 (a &b) M-GITM computed densities binned in the same trajectory as the NGIMS data
530 available from Ls ~180-210 at 200km. The log10 of the density is taken and the difference
531 between the computed densities and the observed NGIMS data is plotted. (a) The difference
532 between the model with gravity waves. The match is very good on the dawn side mid latitudes
533 (2-5h, 0-40^{o}N lat), but the match becomes significant at higher latitudes and night side (22-1h,
534 40-60+^{o}N lat). (b) The difference between the model without gravity waves and NGIMS data. A
535 small relatively good match on the dawn side, and above 50^{o}N latitude, but in general the data-
536 model match is better with the gravity waves than without.
537

538

539 Figure 5

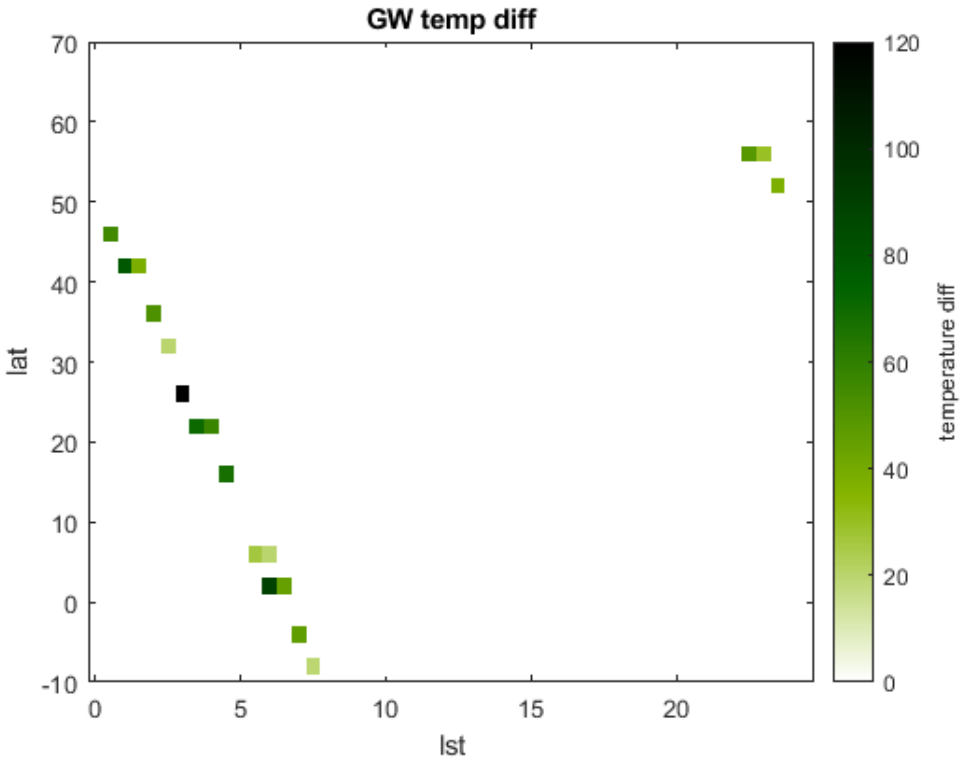

540 (a)

541 (b)

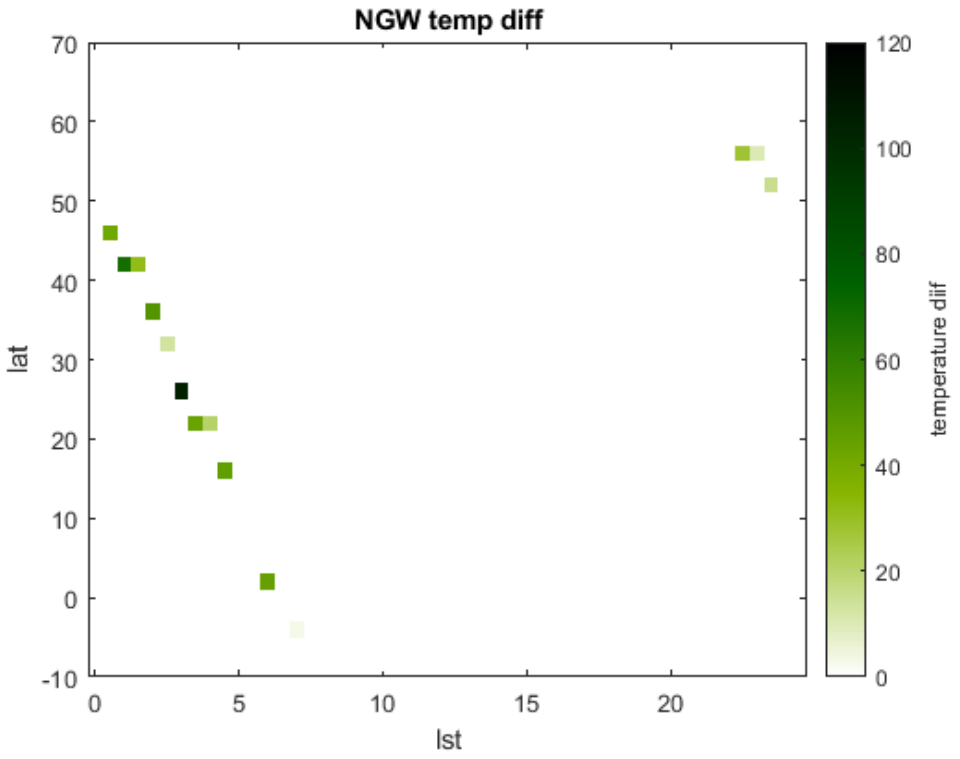

Figure 5 (a&b) M-GITM temperature data binned to correspond to the NGIMS data from Ls ~180-240 during the PEDE. A linear difference between the computed model data and the NGIMS scale height temperature data. (a) The M-GITM model using including gravity waves. (b) the M-GITM model without using gravity waves. Both plots have the same color scale. The temperatures have a slightly better match without the gravity waves at the higher latitudes, but a better match with the gravity waves at the lower latitudes. This gives us some direction for how to modify the gravity waves moving forward during the dust event.

Figure 1a.

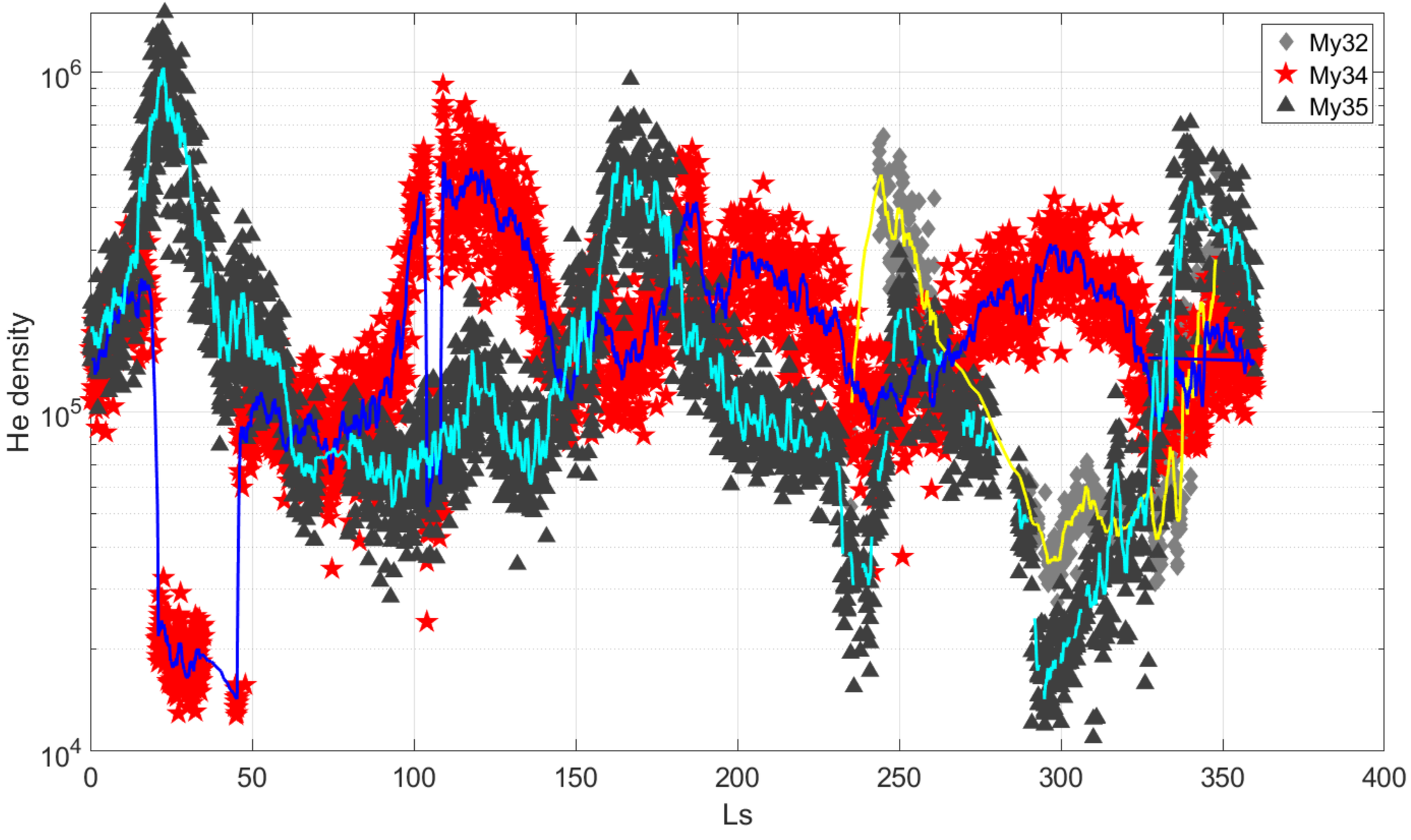
My32
My34
My35
He density
Ls
10^6
10^5
10^4
0
50
100
150
200
250
300
350
400

Figure 1b.

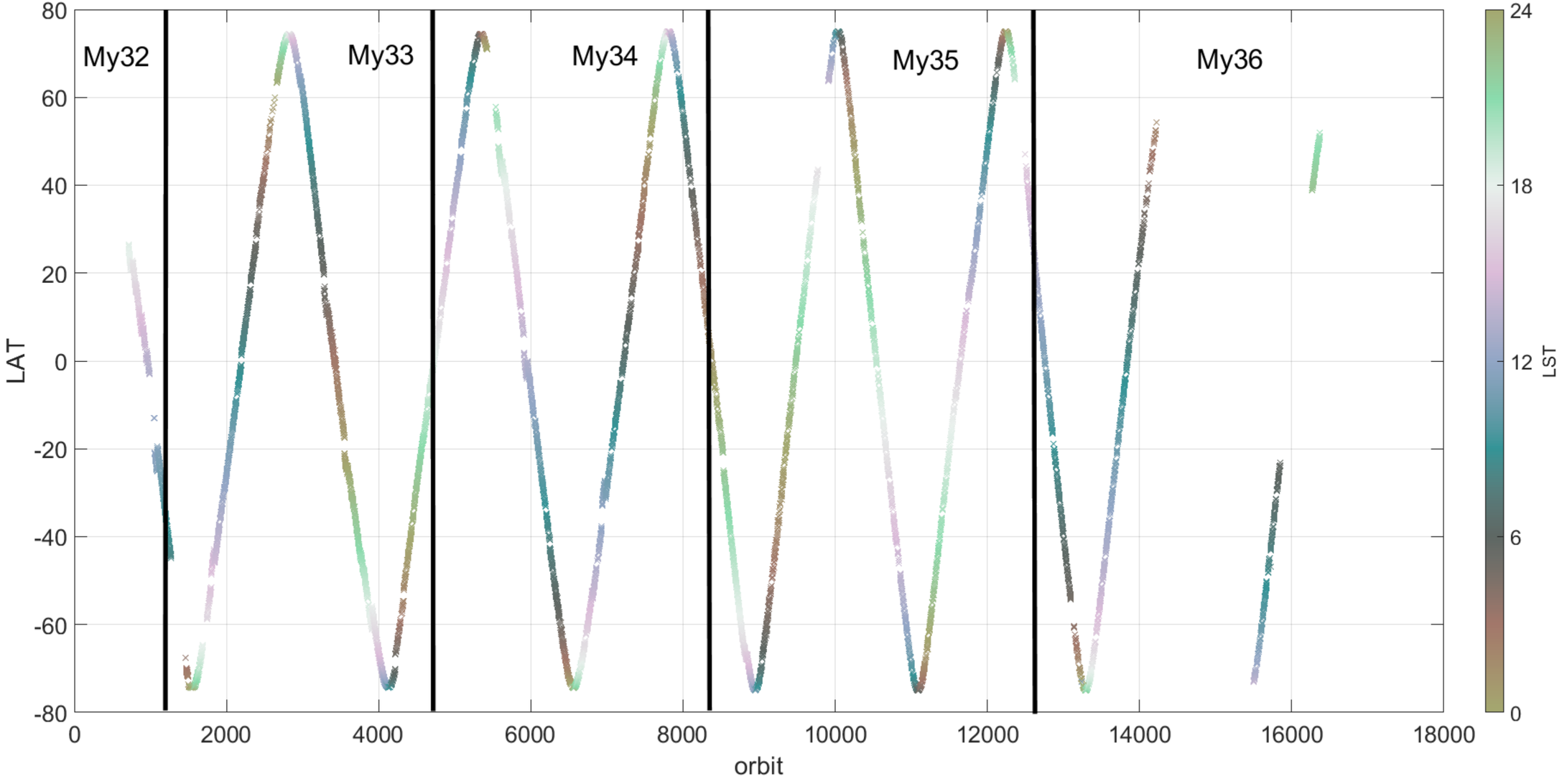
My32
My33
My34
My35
My36
LAT
orbit
LST
80
60
40
20
0
-20
-40
-60
-80
0
2000
4000
6000
8000
10000
12000
14000
16000
18000
24
18
12
6
0

Figure 2a.

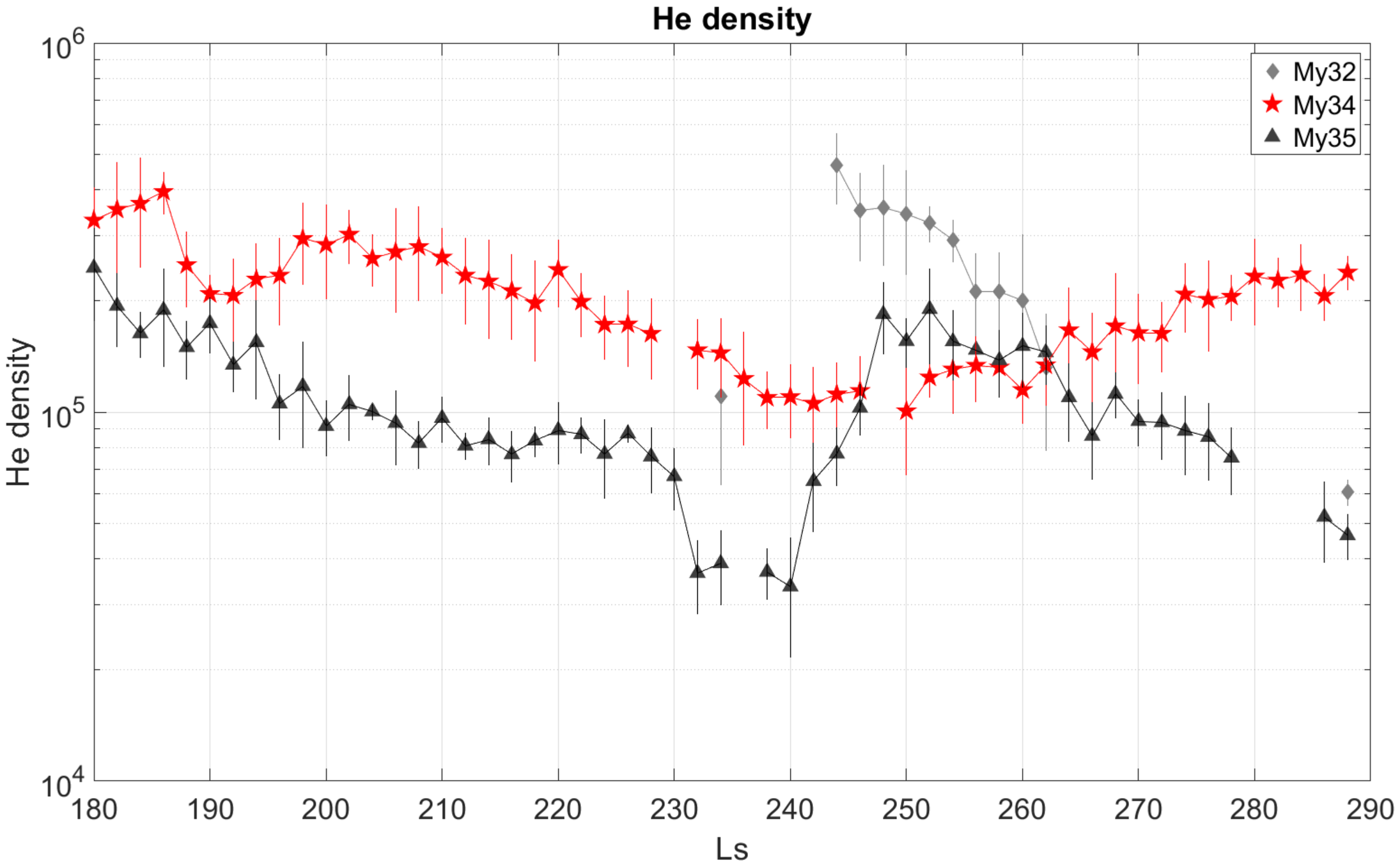
He density
My32
My34
My35
10^6
10^5
10^4
He density
180
190
200
210
220
230
240
250
260
270
280
290
Ls

Figure 2b.

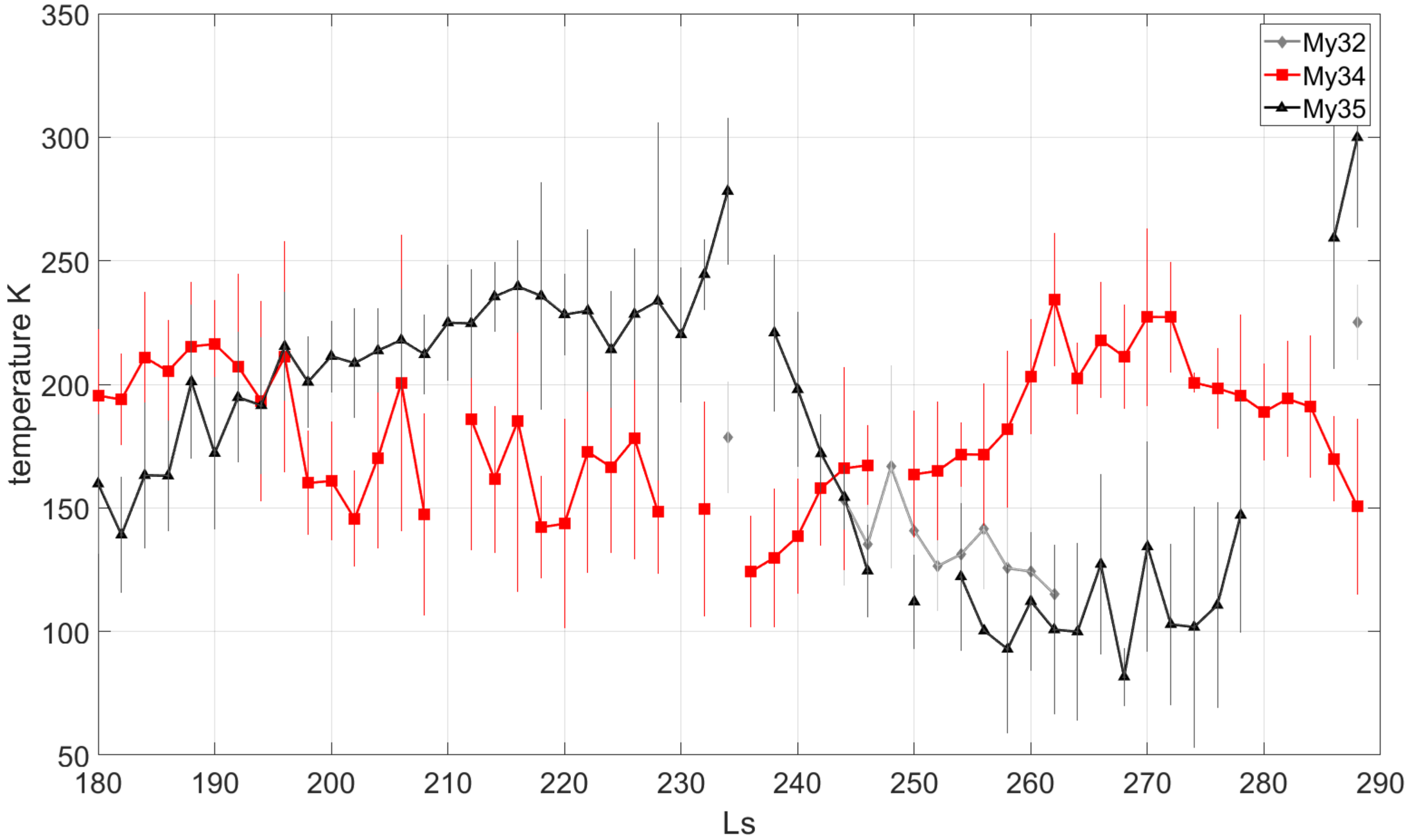
My32
My34
My35
temperature K
Ls
350
300
250
200
150
100
50
180
190
200
210
220
230
240
250
260
270
280
290

Figure 3.

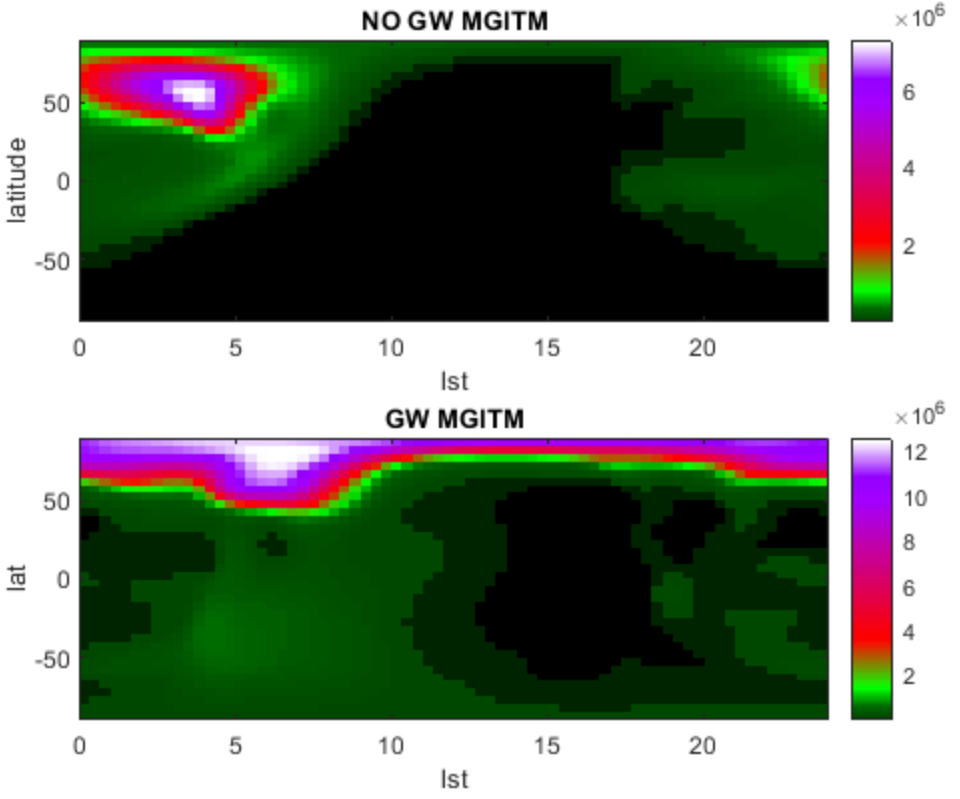
NO GW MGITM
×10^6
6
4
2
50
0
-50
latitude
0
5
10
15
20
lst
GW MGITM
×10^6
12
10
8
6
4
2
50
0
-50
lat
0
5
10
15
20
lst

Figure 4a.

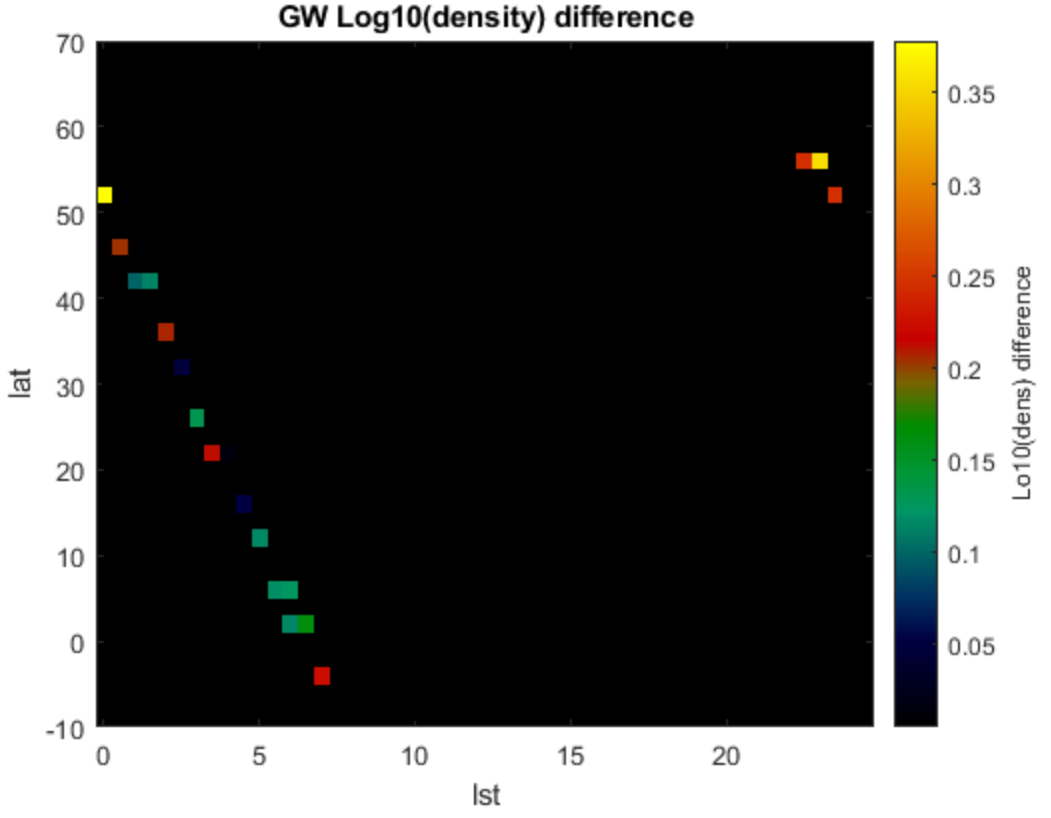
GW Log10(density) difference
70
60
50
40
30
20
10
0
-10
lat
0
5
10
15
20
lst
0.35
0.3
0.25
0.2
0.15
0.1
0.05
Lo10(dens) difference

Figure 4b.

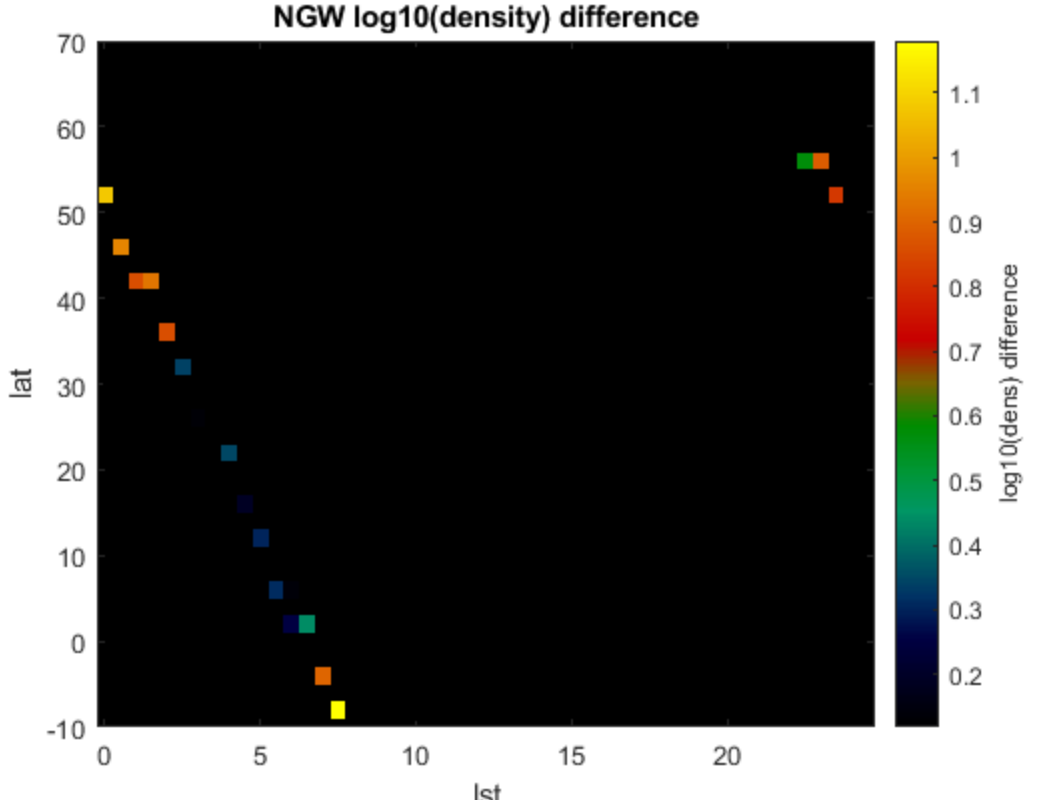
NGW log10(density) difference
70
60
50
40
30
20
10
0
-10
lat
0
5
10
15
20
lst
1.1
1
0.9
0.8
0.7
0.6
0.5
0.4
0.3
0.2
log10(dens) difference

Figure 5a.

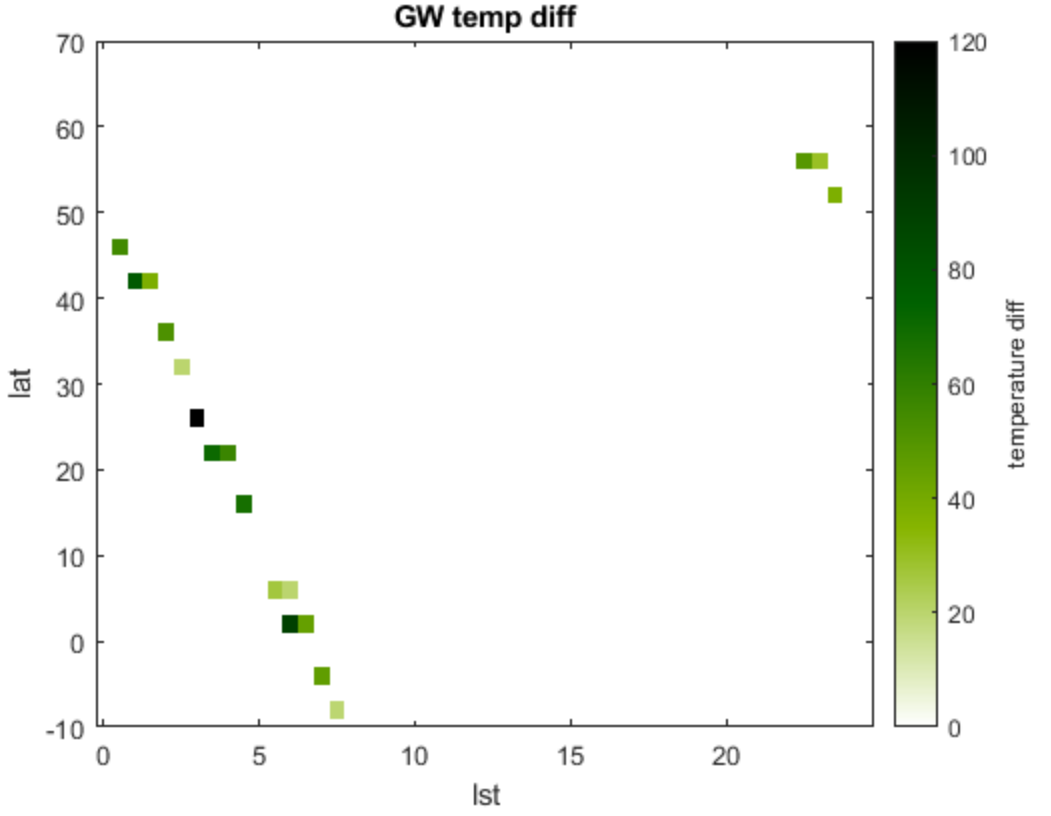
GW temp diff
lat
lst
temperature diff
70
60
50
40
30
20
10
0
-10
0
5
10
15
20
120
100
80
60
40
20
0

Figure 5b.

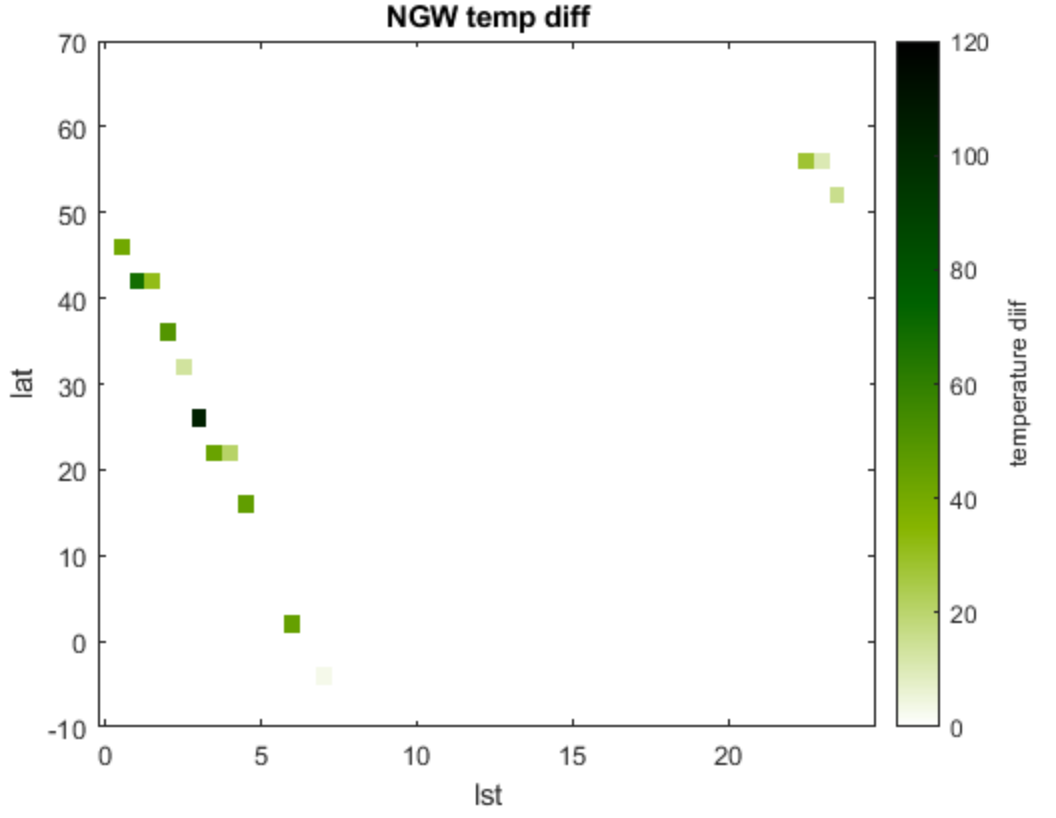
NGW temp diff
70
60
50
40
30
20
10
0
-10
lat
0
5
10
15
20
lst
120
100
80
60
40
20
0
temperature diff